IEEE Access
Multidisciplinary | Rapid Review | Open Access Journal

Received August 14, 2020, accepted August 20, 2020, date of publication August 24, 2020, date of current version September 8, 2020.

Digital Object Identifier 10.1109/ACCESS.2020.3019066

Extension of Quadcopter Flight Range Based on Quadcopter Transport System and Autonomous Ramp Flight Algorithm

CHEONGHWA LEE, SANGWOONG LEE, AND BAEKSUK CHU
Department of Mechanical System Engineering, Kumoh National Institute of Technology, Gyeongsangbuk-do 39177, South Korea
Corresponding author: Baeksuk Chu (bschu@kumoh.ac.kr)

This work was supported by the Technology Advancement Research Program (TARP) Program through by the Ministry of Land, Infrastructure and Transport of Korean Government under Grant 20CTAP-C153093-02.

ABSTRACT In this study, a new method was developed to extend the flight distance of unmanned aerial vehicles such as quadcopters that operate on a limited battery capacity. The suggested method consists of a high-altitude flight initiation system, which uses a carrier rocket, and an autonomous ramp flight algorithm. First, a quadcopter, called a mission quadcopter in this research, is loaded onto the carrier rocket by a folding mechanism, and the rocket flies to a designated height. Then, the carrier rocket releases the mission quadcopter at the high altitude and achieves flight deployment after an unfolding process. Subsequently, the airdropped mission quadcopter stabilizes its pose and flights toward the selected target point. During the flight, it adopts an autonomous ramp flying trajectory. Ramp flying is performed from the sky to the ground surface instead of conventional step shape flying to minimize the flight trajectory and energy consumed while flying. Experiments were performed in Nevada, USA during an international rocket-based airdrop competition, ARLISS (A Rocket Launch for International Student Satellite). The mission quadcopter's real-time latitude, longitude, and altitude were measured to confirm the position information regarding the quadcopter's flight trajectory. The mission quadcopter successfully separated from the carrier rocket, deployed for flight at a high altitude, turned to the target point, performed autonomous ramp flying, and landed.

INDEX TERMS Airdrop, carrier rocket, quadcopter, ramp shape flightpath, foldable wing structure.

I. INTRODUCTION

Currently, numerous researches are actively being conducted on the use of unmanned aircrafts in a variety of fields, such as disaster monitoring, image capturing, logistics, military missions and so on. The unmanned aircrafts, known as drones or multicopters, are widely used to fly quickly and easily through three-dimensional (3D) space with rotary wings. However, multicopters have the disadvantage of only being able to operate within a limited battery capacity, and the technology for replacing multicopter batteries during flight has not yet been developed. This disadvantage limits the operational time and flight distance of multicopters [1]–[13].

Figure 1 shows the conventional solutions to this problem that uses carrying systems to lower the quadcopter's battery consumption and increase its flight radius. Higashino *et al.* (2014) suggested a novel idea of balloon-UAV system for an aerosol observation and sampling [14]. The balloon-UAV system as shown in figure 1(a) is that the balloon carries the UAV, and which keeps up to the target altitude then retrieves the UAV. The UAV is automatically separated from the balloon and return to the ground station. The balloon for carrying can easily reach higher altitude more than 20 km till the balloon breaks up, and it uses density difference so there is not any energy consumption. Thus, the balloon is more handy and inexpensive compare with any other carrying methods. While this method has two critical drawbacks. One is that the balloon does not have controllability so that it makes the balloon the UAV are vulnerable and easily affected from the windy circumstance. Thus, this situation makes instability condition when the UAV release from the balloon. The other is that if the carrying needs fast speed then this balloon method is not appropriate to be adopted. Jo *et al.* (2019) have developed a new equipment

The associate editor coordinating the review of this manuscript and approving it for publication was Dipankar Deb.

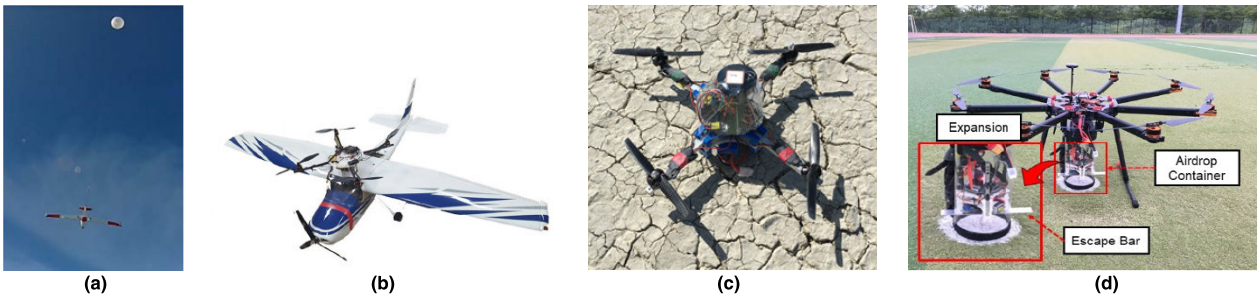

FIGURE 1. Case studies of carrying systems for a unmanned aerial vehicle. (a) A glider unmanned aircraft equipped with a balloon [14]. (b) A fixed-wing unmanned aircraft equipped with a quadcopter [15]. (c) A quadcopter using step flight algorithm [16]. (d) The octocopter equipped with a quadcopter [17].

so that a quadcopter can be automatically deployed by a release system installed on a fixed-wing unmanned aircraft (figure 1(b)) [15]. And, this study analyzed the flight trajectories of the fixed-wing unmanned aircraft and the quadcopter released in the air respectively. However, due to of the difference on flight mechanism between the fixed-wing aircraft and the rotary-wing aircraft, airdrop of the quadcopter from a high-speed fixed-wing unmanned aircraft creates a severe situation for quadcopter pose recovery; 8 seconds or more are required for the quadcopter to recover its pose. Figure 1(c) is from Lee and Chu (2017) that can be considered a precursor to this study [16]. Lee and Chu utilized a carrier rocket and performed rocket-based airdrop experiments in which it ejected a mission drone, in the air during on international airdrop competition, ARLISS (A Rocket Launch for International Student Satellite). Because the flight range of the rocket approached 5 km, the experiments were performed at the Black Rock Desert, Nevada in the United States, which provided a sufficiently large testing environment [18]–[26]. According to the competition's regulations, a limited number of opportunities for flying was given. During the experiments, the quadcopter's real-time latitude and longitude data were collected, but the flight altitude information was not collected, and information enough to describe the quadcopter's flight trajectory was not obtained. An autonomous step shape flight algorithm was adopted to first perform vertical altitude control and then horizontal position control. In the experiment, the quadcopter was controlled up to the desired altitude, but it made an emergency landing during the autonomous flight to the target point due to insufficient battery caused by excessive energy consumption while performing altitude control. Lee *et al.* (2019) performed an experiment in which the carrier rocket was exchanged to a large octocopter (figure 1(d)) [17]. After the octocopter was used to perform the primary flight, the separated quadcopter performed the secondary flight to extend the flight distance.

In the present study, a new method of extending the flight distance of quadcopters within the limit capacity and operating times of the batteries was developed. This method was verified by autonomous flight experiments in which a high-altitude flight deployment mechanism that employs a carrier rocket was adopted, and a ramp path was used to shorten the battery consumption time. For the high-altitude flight deployment mechanism, a mission quadcopter was put inside a carrier rocket that has a long flight distance, and the carrier rocket's energy source was consumed first to fly for a long distance. After the carrier rocket's energy was entirely consumed, the mission quadcopter separated from the carrier rocket and the mission quadcopter's own energy was consumed to continue the flight. In the autonomous ramp flight algorithm, the mission quadcopter that has come out of the carrier rocket performs consecutively pose control and flies a ramp flight trajectory that minimizes energy consumption to the chosen target point with the help of position and altitude information from a GPS sensor and barometer, and then land. This paper reports the follows: (1) the structure of the rocket which is used as a carrier rocket, (2) the design of the quadcopter which has a foldable structure in which the wing frame folds to fit inside an airdrop containers, and (3) the algorithm by which the quadcopter separates from the rocket, which has been shot 3 km into the sky, and then initiates flight at a high altitude and autonomously flies to the target point.

The remainder of this paper is structured as follows. Section 2 describes the separated structure of the carrier rocket, the foldable structure of the mission quadcopter, the system's overall operating algorithm, and the detailed airdrop mechanism that is needed for the high-altitude deployment. Section 3 describes the basic control system of the mission quadcopter, which uses a fundamental flight control algorithm, and the step shape flight and ramp shape flight algorithms are demonstrated. Section 4 discusses the experiments conducted to verify the high-altitude flight initiation system and the ramp flight trajectory until at the chosen target point. Section 5 describes the concluding remarks regarding the high-altitude flight initiation using a carrier rocket and an autonomous flight algorithm.

II. CONFIGURATION OF QUADCOPTER TRANSPORT SYSTEM USING A ROCKET AND A FOLDABLE QUADCOPTER

A. HIGH-ALTITUDE TRANSPORT MECHANISM AND STRUCTURE OF A CARRIER ROCKET AND A FOLDABLE QUADCOPTER

The exterior and interior structure of the carrier rocket used in this study are shown in figures 2(a) and 2(b), respectively.

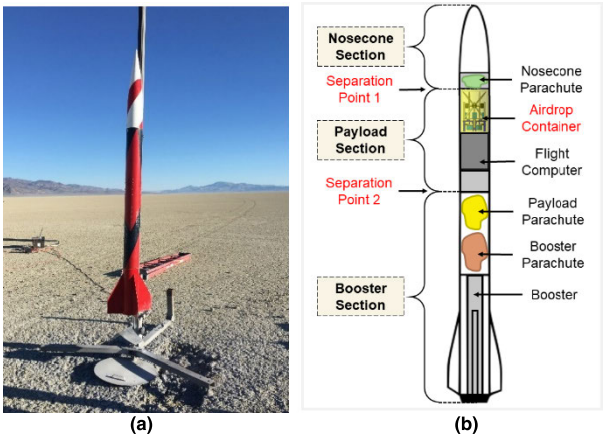

FIGURE 2. Exterior and inner structure of the carrier rocket. (a) Exterior view of the carrier rocket. (b) Inner structure of the carrier rocket.

The rocket is divided into the nosecone section, which is the conical front part that reduces air resistance; the payload section, which contains the airdrop container and the main controller; and the booster section, which contains the booster, the rocket's power source. The foldable quadcopter is located in the airdrop container. When the payload section separates from the nosecone section at separation point 1, the foldable quadcopter is ejected at a high altitude from the airdrop container. The carrier rocket separates into three pieces at separation points 1 and 2, and they return safely to the ground with the help of parachutes. The carrier rocket's diameter is 152 mm, and its height is 2794 mm. Its allowable payload is 1.8 kg, and the airdrop container within the rocket has a width of 150 mm and a height of 250 mm (Table 1).

The payload in the carrier rocket is the foldable quadcopter, which has four rotary wings. Figure 3 shows the appearance of the foldable quadcopter loaded in the airdrop container. When the foldable quadcopter's wing frame is unfolded, it has a diameter of 360 mm and a height of 90 mm; it has a wide diameter and a low height (figure 3(a)). However, the carrier rocket's airdrop container has a diameter of 150 mm and a height of 250 mm, which is relatively narrow and long. Therefore, to load the foldable quadcopter into the airdrop container, which has limited space, the quadcopter's wing frame is folded as shown in figure 3(b) and it is loaded into the carrier rocket's airdrop container as shown in figure 3(c).

TABLE 1. Specifications of the carrier rocket and the foldable quadcopter.

Aircraft		Diameter (mm)	Height (mm)	Weight (kg)
Carrier rocket		152	2794	35.00
Airdrop container		150	250	0.36
Foldable quadcopter	Unfolded	360	90	0.61
	Folded	132	210	

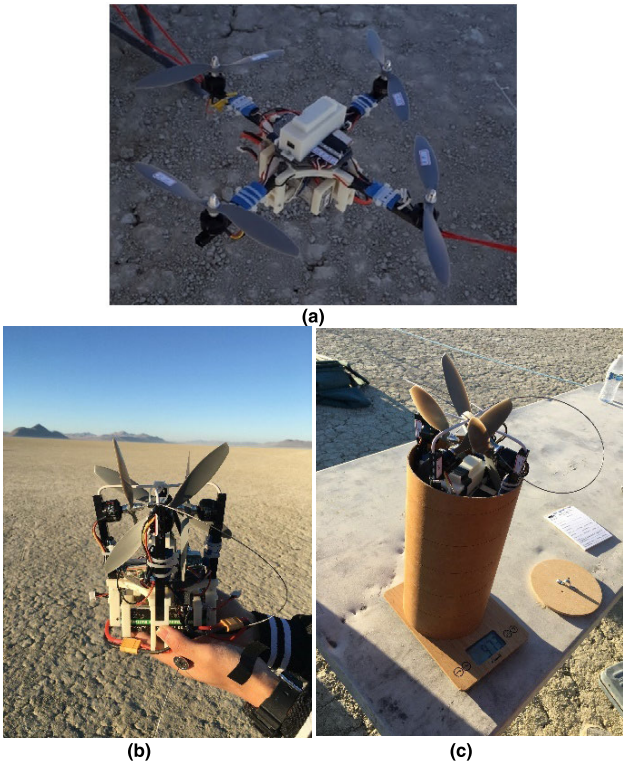

FIGURE 3. Foldable structure and inserted view of the foldable quadcopter. (a) Unfolded view of the foldable quadcopter. (b) Foldable view of the foldable quadcopter. (c) Inserted view in the airdrop container.

When its wing frame is folded, the foldable quadcopter has a diameter of 132 mm and a height of 210 mm, and it can be loaded into the airdrop container. The foldable quadcopter's weight is 0.61 kg. Because the foldable quadcopter's weight is lighter than the carrier rocket's allowable payload weight of 1.8 kg, the experiments could be performed with the carrier rocket. Table 1 shows the diameter, height, and weight of the carrier rocket, airdrop container, foldable quadcopter with wing frame unfolded, and foldable quadcopter with wing frame folded.

B. HIGH-ALTITUDE TRANSPORT FLIGHT PROCEDURE USING THE ROCKET

Figure 4 gives an overview of the experiment conducted to test the high-altitude flight initiation and autonomous flight algorithm to verify the rocket-based high-altitude transport system from the preparation stage to landing. (1) The carrier rocket is loaded with the foldable quadcopter and preloaded at the rocket launching point. (2) After flight preparations are completed, the carrier rocket is launched, and the quadcopter is transported into the sky to an altitude of 3.0∼3.5 km. (3) The rocket separates into three pieces, and the quadcopter is ejected into the air. (4) The separated carrier rocket sections use individual parachutes to safely land on the ground, and the ejected quadcopter automatically unfolds its wing frame at a high altitude. After 5 seconds of freefall, a flight initiation signal is sent and four wing motors are activated.

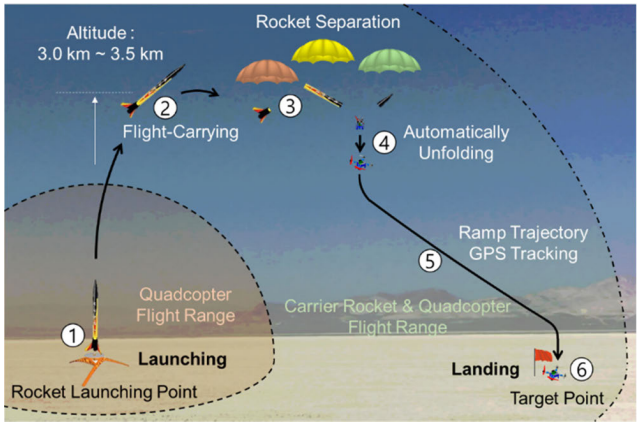

FIGURE 4. High-altitude transport flight procedure.

During freefall, the mission quadcopter tries to establish pose control. There exists a possibility that the quadcopter, which is ejected from the carrier rocket, could collide with the carrier rocket if it begins to fly immediately after ejection. In order to prevent this, it freefalls for a fixed time of 5 seconds and then recovers its pose and begins to fly. The quadcopter goes through a process of establishing a pose for a fixed time. (5) Then, the quadcopter maintains a stable pose and uses ramp trajectory GPS tracking to fly the shortest distance to the designated target point's GPS location. It performs altitude and planar control simultaneously and minimizes battery consumption. (6) When the quadcopter arrives at the target point, it reduces its motor power and ends the flight by landing.

III. AUTONOMOUS FLIGHT ALGORITHM OF THE QUADCOPTER

A. FUNDAMENTAL FLIGHT CONTROL ALGORITHM

The mission quadcopter is controlled by the fundamental flight control algorithm, which is based on the proportional-integral-differential (PID) control method and Quad-X type kinematics (MultiWii 2019) [27]. This control algorithm provides altitude control, planar control, and landing function. The control algorithm acquires the altitude information (z) from the barometer installed in the inertia measurement unit (IMU) sensor to perform altitude control, and it obtains the latitude (x) and longitude (y) information through the GPS to perform planar control. A PID-based control algorithm is used for the quadcopter's flight control and pose control (figure 5). The PID-based control algorithm is divided into the altitude control, which controls z component among the three-dimensional position parameters (x, y, z), and the planar control, which controls x and y components. The altitude control is performed as follows. The difference between the preset altitude value (z_{set}) and the current altitude value (z_{real}) measured by the IMU sensor are inputted into the PID-based controller, and the altitude control signal (u_δ) is generated [28], [29]. However, for an autonomous ramp flight, a novel altitude planer is added in this study, which will be described in section III.B. The command signal of the for planar control flying toward the target point is calculated using the target point's GPS values (x_{set}, y_{set}) that were preset at the beginning of flight and the current values (x_{real}, y_{real}) collected by the quadcopter's GPS module in real time. This position information goes through the pose generator in figure 5 and is converted into a 3D pose signal i.e. roll, pitch, and yaw (ϕ_{cmd}, θ_{cmd}, ψ_{cmd}) and a distance signal (d_{real}). The pose signal is compared with the quadcopter's actual pose signal (ϕ_{real}, θ_{real}, ψ_{real}) that was measured using the IMU sensor in Eqs. (1) to (3)

$$\Delta\phi = \phi_{cmd} - \phi_{real} \tag{1}$$
$$\Delta\theta = \theta_{cmd} - \theta_{real} \tag{2}$$
$$\Delta\psi = \psi_{cmd} - \psi_{real} \tag{3}$$

where the error signals entered in the PID/PI-based controller to produce the planar control signal (u_ϕ, u_θ, u_ψ) shown in Eqs. (4) to (6). The altitude control signal (u_δ) will be covered in section III.B.

$$u_\phi = P_\phi \Delta\phi + I_\phi \int \Delta\phi dt + D_\phi \frac{d\Delta\phi}{dt} \tag{4}$$
$$u_\theta = P_\theta \Delta\theta + I_\theta \int \Delta\theta dt + D_\theta \frac{d\Delta\theta}{dt} \tag{5}$$
$$u_\psi = P_\psi \Delta\psi + I_\psi \int \Delta\psi dt \tag{6}$$

where the uppercase of Ps, Is, and Ds are the proportional, integral, and derivative gain parameters, respectively. All of the gain parameters are determined as constant values. In details, P_ϕ and P_θ are 3.3, P_ψ is 6.8, I_ϕ and I_θ are 0.03, I_ψ is 0.045, D_ϕ and D_θ are 23. The control signals generated by the altitude control and the planar control are entered into the quadcopter's inverse kinematics formulas and used to calculate the motor's output signals m_1, m_2, m_3, and m_4. The quadcopter inverse kinematics are expressed in Eq. (7). The rightest block at figure 5 shows the quadcopter's wing positions with quad-X structure and specifies which motors are m_1, m_2, m_3, and m_4. In the block, arrow direction is the quadcopter's forward direction.

$$\begin{Bmatrix} m_1 \\ m_2 \\ m_3 \\ m_4 \end{Bmatrix} = \begin{bmatrix} +1 & -1 & -1 & +1 \\ -1 & -1 & +1 & +1 \\ -1 & +1 & -1 & +1 \\ +1 & +1 & +1 & +1 \end{bmatrix} \begin{Bmatrix} u_\phi \\ u_\theta \\ u_\psi \\ u_\delta \end{Bmatrix} \tag{7}$$

B. AUTONOMOUS STEP AND RAMP FLIGHT ALGORITHM WITH AN ALTITUDE PLANER

The quadcopter's autonomous step flight algorithm draws a step shape flight path for autonomous flying because altitude control (z) and planar control (x, y) are performed separately. The autonomous step flight algorithm first performs the altitude control to descend while maintaining latitude and longitude until it arrives at the preset flying altitude (z_{set}) (the dotted path in figure 6). When the quadcopter arrives at the preset flying altitude, the planar control is executed and the quadcopter flies while maintaining the altitude until the latitude and longitude positions are reached within the

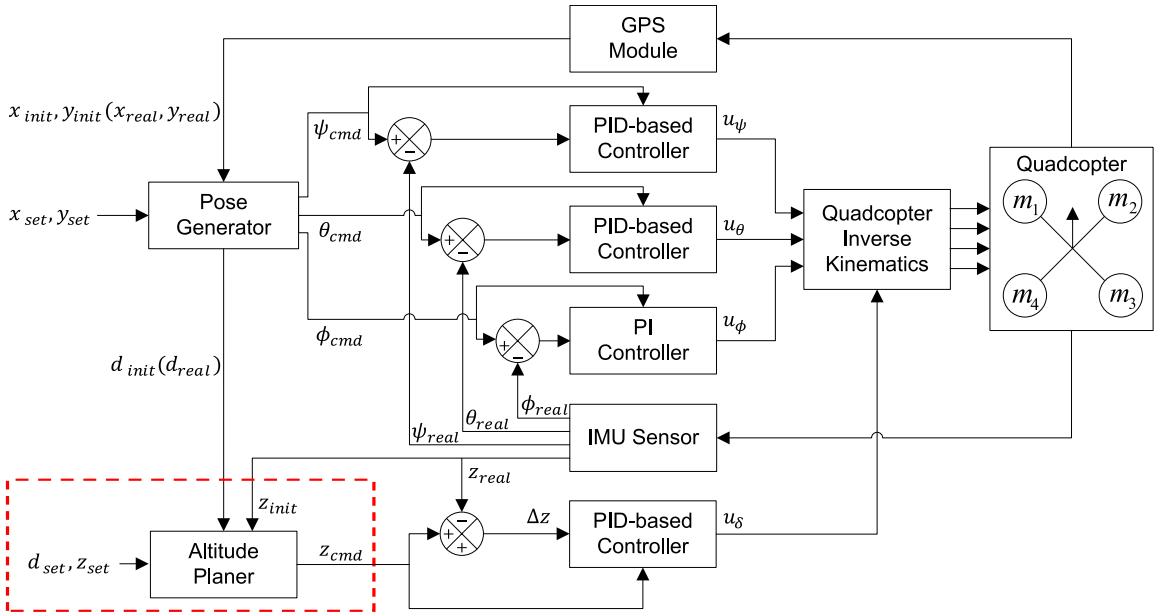

FIGURE 5. PID-based flight control algorithm for the mission quad-copter.

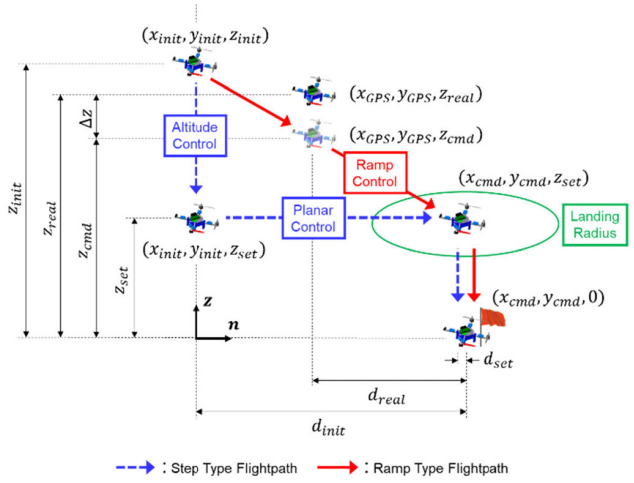

FIGURE 6. Step and ramp shape flightpath of the mission quadcopter [16].

landing radius. When it has arrived into landing radius, the quadcopter pauses in the air for 5 seconds and goes through a process of checking various settings needed to land such as hovering and flying altitude. Then, it descends to land and ends the autonomous flight. The autonomous step flight algorithm can be used without any problems when the flight distance is short, but as the flight distance becomes longer, the algorithm uses the battery less efficiently. Because the autonomous step flight algorithm performs planar control sequentially after altitude control, the flight trajectory becomes longer, causing a problem in which the flight time is extended, battery consumption is increased, and the quadcopter's operating efficiency is decreased [30]–[37].

In this study, an autonomous ramp flight algorithm in which altitude control (z) and planar control (x, y) are performed simultaneously was developed to fly along the shortest distance between the departure point and the arrival point. The autonomous ramp flight algorithm is the solid line path shown in figure 6 Compared to the autonomous step flight algorithm, the autonomous ramp flight algorithm has a relatively short flight path because the altitude planner is added to the existing autonomous step flight algorithm to perform the altitude control at the planar control stage. The altitude planner is located on the dotted box in figure 5. The altitude planner uses a map function to output the altitude command value (z_{cmd}) required for altitude control. The formula used in the map function is in Eq. (8):

$$\begin{aligned} z_{cmd} &= map\,(d_{real}, z_{set}, z_{init}, d_{set}, d_{init}) \\ &= \frac{z_{init} - z_{set}}{d_{init} - d_{set}} d_{real} + z_{set} \end{aligned} \tag{8}$$

where z_{set} and z_{init} as well as d_{set} and d_{init} are used to determine the ramp angle for the quadcopter flight. The z_{set} and d_{set} are vertical and horizontal positon values where the landing can be initiated in the landing radius and are initially set to 100 and 0 meters during the flight preparation stage, respectively. z_{init} is the altitude measured by the IMU sensor at the initial time point when the ramp landing begins, and d_{init} is the distance calculated by inputting the x_{init} and y_{init} values measured by the GPS into the pose generator. d_{real} refers to the real-time distance from the quadcopter's current location to the target point as measured by the GPS sensor. If d_{real} is inserted to the map function, z_{cmd} is outputted as a control signal. For example if z_{set}, z_{init}, d_{set}, and d_{init} in Eq. (8) (map function) are 0, 1000, 0, and 3000, respectively, and a value of 2400 is used as d_{real}, a z_{cmd} value of 800 is outputted, which is the altitude relative to the distance. Then, the quadcopter, at the current real-time altitude (z_{real}), flies

toward the given control signal altitude (z_{cmd}). The altitude command signal produced by the map function (z_{cmd}) is sent to the PID-based controller together with the actual altitude signal (z_{real}), where they are processed based on the PID formula, Eq. (9), to generate the quadcopter's output control signal (u_δ) in Eq. (10). Therefore, as the distance between the target point and the quadcopter decreases, the altitude decreases proportionally, and a ramp shape flight path is created.

$$\Delta\delta = z_{cmd} - z_{real} \tag{9}$$

$$u_\delta = P_\delta \Delta\delta + I_\delta \int \Delta\delta dt + D_\delta \frac{d\Delta\delta}{dt} \tag{10}$$

where P_δ is 6.4, I_δ is 0.025, and D_δ is 24. Since during the ramp flight, there is a danger of crashing in case of a steep descent. The ramp's slope command was limited to less than 35°.

IV. QUADCOPTER TRANSPORT AND AUTONOMOUS RAMP FLIGHT EXPERIMENTS

A. PRELIMINARY EXPERIMENT FOR AUTONOMOUS RAMP FLIGHT ALGORITHM

For the quadcopter to fly safely, it is necessary to adjust the control parameters through several rounds of manual and autonomous flight testing. The control parameters are affected not only by the quadcopter's own kinetic characteristics such as weight and moment of inertia, but also by external factors such as atmospheric pressure, temperature, and wind. In the Black Rock Desert in Nevada, United States, where the ARLISS competition was held, the flight environment differs from that in South Korea, and it was necessary to set new control parameters. In the ramp flight algorithm, the starting height was set at 150 meters, and the flying distance to the target point was set at 250 meters. Two local preliminary tests were performed. The first local preliminary test measured the landing distance error, which is the distance from the quadcopter's landing point to the target point. The landing distance error was 19.08 meters (figure 7(a)(1)) owing to the effects of the desert testing environment with strong winds and a large amount of dust during landing vertically after the quadcopter's autonomous flight. In the second test, the power was increased in response to the local environment to overcome the effects of the wind and reduce the error. The parameters were set, and the autonomous ramp flight test was performed again at the same altitude and flight distance. As shown in figure 7(a)(2), the error was 1.27 meters. Figure 7(b) shows the 3D flight path according to the quadcopter's latitude, longitude, and altitude in both tests. Table 2 shows the GPS coordinates of the tests' target point, initial flight altitude, initial flight distance, flight time, and the landing distance error from the target point. The target point is designated by the ALRLISS committee as (40.879694, –119.121806) which are longitude and latitude, respectively. Note that the proposed algorithm can land at any point.

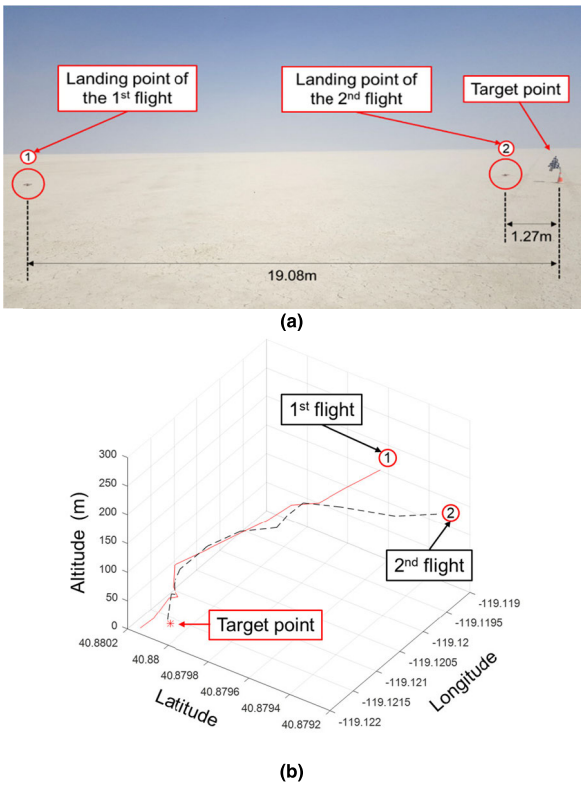

FIGURE 7. Preliminary tests for the autonomous ramp flight. (a) Landing points of the preliminary tests. (b) 3D flight trajectory of the preliminary tests.

TABLE 2. Results of the preliminary autonomous ramp flight tests.

Category	Test 1	Test 2
GPS position	Target point (40.879694, –119.121806)	
GPS sampling time	6 s	
Initial flight altitude	150 m	
Initial flight distance	250 m	
Flight time	72 s	78 s
Landing distance error from the target point	19.08 m	1.27 m

B. HIGH-ALTITUDE TRANSPORT AND AUTONOMOUS RAMP FLIGHT EXPERIMENT PREPARATION PROCESS

The high-altitude flight initiation and autonomous flight experiment requires a special experimental setting in which a carrier rocket and a mission quadcopter are launched to a height of 3 km. However, it is difficult to create such an experimental setting in South Korea owing to aviation laws and safety issues. Therefore, we participated in the ARLISS competition, which provided the experimental setting needed to test the high-altitude flight, i.e., two opportunities to experiment with high-altitude flight initiation and autonomous flight. During one of the two experiments, the quadcopter crashed owing to a device malfunction during freefall, and

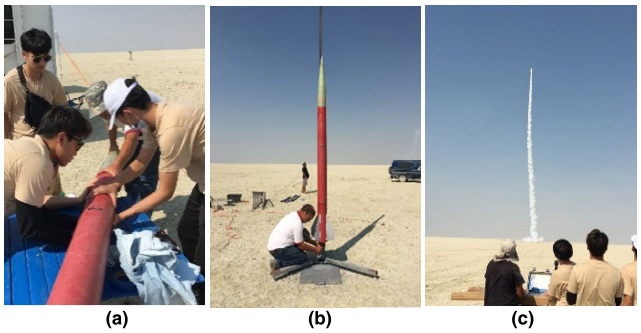

FIGURE 8. Procedure to launch the carrier rocket. (a) Assembling the carrier rocket. (b) Preparation for launching. (c) Launching.

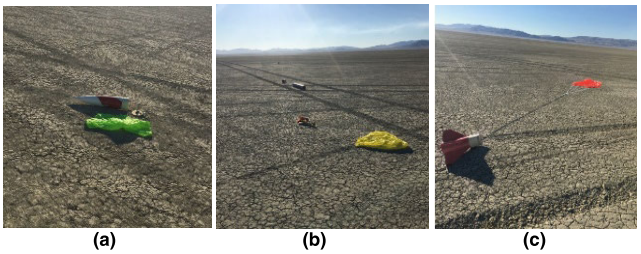

FIGURE 9. Carrier rocket sections with parachutes after landing on the ground. (a) Nosecone section. (b) Payload section. (c) Booster section.

it was not possible to obtain viable results. Therefore, the second experiment was conducted and the following results were obtained.

Figure 8 shows the sequential process of preparing for the high-altitude flight initiation experiments: place the quadcopter into the airdrop container, load it into the carrier rocket, and launch it. In figure 8(a), the target point's GPS position is inputted before loading the mission quadcopter into the carrier rocket, and the EZ GUI status monitoring and the parameter setting tool are used to check that the IMU sensors and the GPS module are working properly. The carrier rocket was assembled after folding the quadcopter's wing frame and placing it in the airdrop container. The assembled carrier rocket was taken to the chosen launch point and set up on the launcher (figure 8(b)). The carrier rocket was launched as shown in figure 8(c), and the high-altitude flight initiation experiment started.

The carrier rocket was launched into the air and successfully separated. Parachutes were used to return the sections to the ground without damage (figure 9). Figures 9(a), (b), and (c) show the nose section, airdrop container, and payload sections, and the booster section on the ground, respectively, along with the parachutes for preventing damage during the fall.

C. EXPERIMENTS FOR HIGH-ALTITUDE TRANSPORT USING A ROCKET AND AUTONOMOUS RAMP FLIGHT

The main objective of the experiments was to initiate the quadcopter flight at a high altitude, fly it to the target point, achieve safe landing, and measure the flight record. To accomplish this mission, five steps must be successfully accomplished. (1) The quadcopter, ejected at a high altitude, must successfully unfold its folded wing frames. (2) The pose control for roll, pitch, and yaw directions must be performed in the air. (3) Autonomous ramp flight must be performed to obtain the shortest flight path to the target point. (4) The main controller's internal memory (EEPROM) must store the quadcopter's altitude and GPS information to confirm the flight path. (5) On arrival over the target point, the quadcopter must safely land.

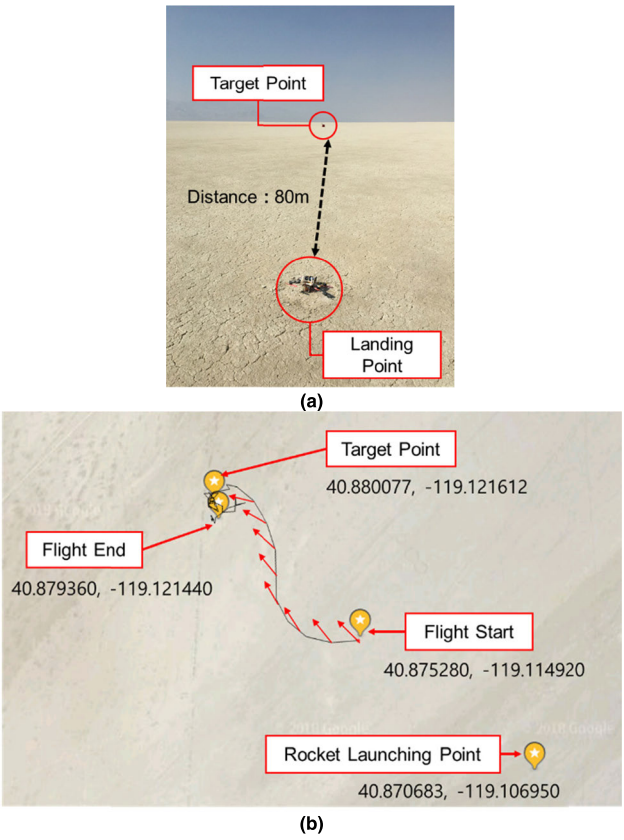

FIGURE 10. Experimental result of autonomous flight based on GPS records. (a) Landing point view of the mission quadcopter. (b) Flight trajectory stored in the EEPROM.

The autonomous ramp flight algorithm suggested in section III. was employed to perform the flight experiments. After separating from the payload airdrop container and flying to the target point and landing, the quadcopter appeared to be whole without any broken components (figure 10(a)). The quadcopter was discovered at a landing point 80 meters away from the target point. To confirm that an accurate quadcopter flight recording was made, the GPS position data stored in the internal EEPROM were checked. Figure 10(b) shows the quadcopter's GPS flight record, which displays the latitude and longitude data stored in the controller's EEPROM. The GPS flight record consists of the flight start and end points and the flight trajectory. The position information was stored in the EEPROM at 6 seconds intervals. The quadcopter began

flying at the flight initiation point and carried out a GPS tracking flight of 700 meters toward the target point for 4 minutes and 42 seconds, collecting 48 data points. Afterward, the GPS position data stored in the EEPROM did not move from the flight end point, and the quadcopter was discovered at the last recorded point in the dataset. The remaining battery voltage was 10.7 V.

Figure 11(a) shows the 3D ramp flight path of the autonomous flight experiment. The figure shows a ramp flight

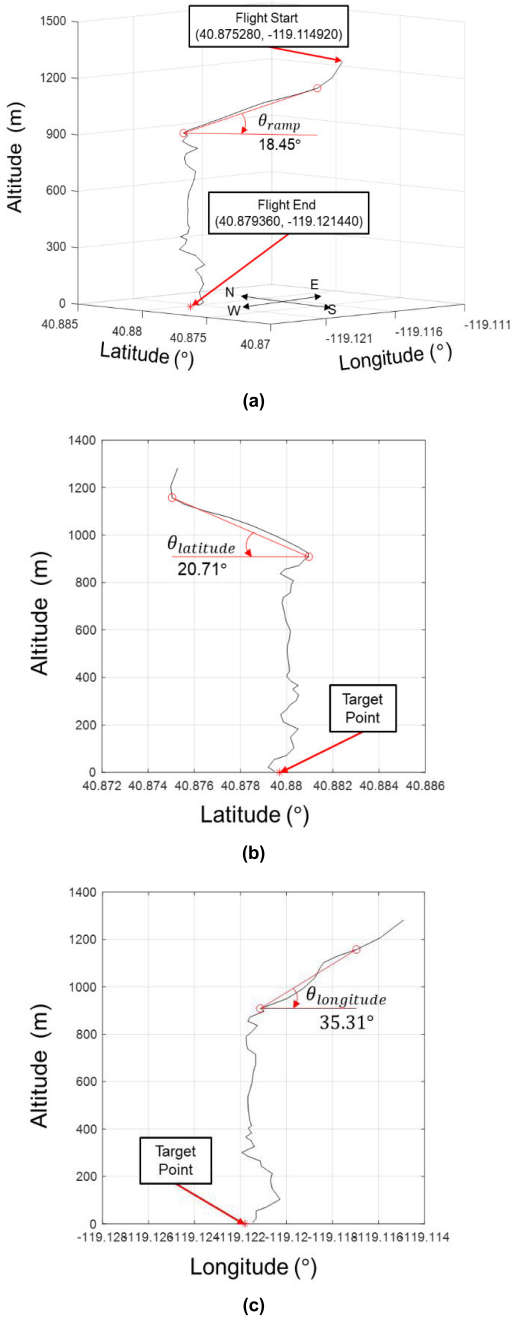

FIGURE 11. Experimental results of the autonomous ramp flight trajectory. (a) 3D view. (b) Latitude and altitude view. (c) Longitude and altitude view.

TABLE 3. Results of the autonomous ramp flight experiment.

Category	Results
GPS position	Target point (40.879694, –119.121806)
GPS sampling time	6 s
Initial flight altitude	1.2818 km
Flight distance	0.7116 km
Flight time	282 s
Landing distance error from the target point	0.08105 km

in which altitude control and planar control were performed simultaneously until the quadcopter arrived over the target point. Figures 11(b) and 11(c) show the flight altitude path according to the quadcopter's latitude and longitude information, respectively. The description of the flight experiment is based on the exterior appearance of the quadcopter discovered at the landing position, the GPS flight records stored in the EEPROM, and the remaining battery life measured directly after discovery. The quadcopter was launched together with the rocket and it successfully separated from the rocket. The wing frame automatically unfolded, and the high-altitude flight was initiated. Following the planned autonomous ramp flight algorithm, it successfully flew down to the target flight altitude at a $\theta_{ramp} = 18.45°$ angle. It performed the autonomous flight with GPS tracking toward the target point. The battery was used efficiently until the autonomous flight was performed, and the target was reached. The flight experiments confirmed the possibility of implementing the quadcopter structure with a foldable mechanism and the autonomous ramp flight algorithm proposed in this study. Table 3 shows the GPS position, GPS sampling time, flight altitude, initial flight altitude, flight distance, flight time, and the landing distance error.

D. COMPARISION WITH OTHER RESEARCHES

A variety of research cases for extending the flight distance of UAVs using a rocket is tabulated in the Table 4 [38]–[44]. All the experiments are carried out under the same fixed conditions. One is that only the rocket is allowed as a carrier, and the other is that the launch point of the rocket is (40.87063, −119.106950) and the target point of the UAV is (40.879694, −119.121806) by ARLISS committees. Additional and detailed conditions of the experiment are contained in a document provided by ARLISS [45]. The metrics for comparison experiment results are the distance between the UAV's actual landing point and the target point, and damages on the UAV. Table 4 summarizes all the results of each team's experiments. Each team selected one of three types of UAV: parafoil, glider, and quadcopter. Each study case has a different folding mechanism for each rocket, a control

TABLE 4. Comparison of the distance error with previous researches.

No.	University	UAV Type	Distance Error (m)	Damage Status	ARLISS Participating Year	Participating Nation
1	University of Tokyo, [38]	Parafoil	3632	Some	2012	Japan
2	Tokyo Metropolitan University, [39]	Parafoil	1786	Some	2013	Japan
3	Soka University, [40]	Glider	1590	Most	2010	Japan
4	University of Nevada, Reno, [41]	Glider	2800	Most	2014	USA
5	University of Tokyo, [42]	Glider	900	None	2018	Japan
6	Georgia Institute of Technology, [43]	Quadcopter	800	Some	2013	USA
7	Kumoh National Institute of Technology, [44]	Quadcopter	1329	Most	2016	Korea
8	Kumoh National Institute of Technology, [16]	Quadcopter	1800	None	2017	Korea
9	Kumoh National Institute of Technology	Quadcopter	81	None	2018	Korea

algorithm for returning to its destination, and the hardware used by sensors, MCU, etc.

A parafoil-type UAV is a UAV that flies using an airfoil-type parachute. Unlike other types of UAV, the parafoil-type UAV does not require folding mechanism because it is built to match the carrier rocket container size. The key developments of parafoil-type UAV are parafoil open mechanism and parafoil control algorithms when it is released from the rocket. It have high stability in protecting aircraft by drag force (air resistance) using parachute even when the UAV is out of control and free fall. However, there is some drawbacks that it is difficult to control to the desired destination due to low controllability because it is easily affected by external conditions such as wind. Team NASU of University of Tokyo (2012) took a strategy of opening parafoil after 25 seconds of free fall to avoid severe wind condition at a high altitude [38]. The UAV recorded 3,632 meters of distance error due to strong wind at the low altitude. Team TBY of Tokyo Metropolitan University (2013) was equipped with propellers to address the parafoil drawbacks and recorded a distance error of 1,786 meters [39].

A glider-type UAV is a UAV that flies without a power unit (e.g. rotors). Glider-type UAVs have the advantages of having high energy efficiency using wide wing spans and controllability using steering devices such as rudder. However, to load a glider-type UAV onto a rocket container, it has wings and fuselage folding or flexible structures and requires unfolding or unrolling mechanism after being ejected from the rocket. Team Kuro-kids of Soka University (2010) was manufactured by folding the wings and body of the UAV in two layers for placing in the container of the rocket [40]. The UAV was found at 1590 meters with most of the body of the UAV being damaged. Because the UAVs do not have one wing unfolding, it seems to have been freefall immediately after failing to control the UAV properly. Smith *et al.* of University of Nevada (2015) developed a glider which has a four-isolated fuselage mounted on a container wrapped in a flexible thin airfoil wing [41]. The UAV carried out a successful unfolding mechanism, but it was found at the distance error of 2800 meters. The rudder was broken due to the impact during the landing process. It was caused by the inappropriate posture controls and errors in GPS data. Team The Wright Staff of University of Tokyo (2018) developed a glider [42]. The distance error was recorded 900 meters.

The quadcopter-type UAV is the UAV that takes off, lands, and flies with four rotors (rotating wings or propellers). Quadcopter has the advantage of being able to fly over windy conditions using multiple rotors. However, more sophisticated manufacturing and control are needed because the UAV can fail to fly even if one of the rotors breaks down. In addition, the quadcopter also needs to be developed folding structure for loading on the rocket and mechanism that unfolding after being released. AlSaibie *et al.* of Georgia Institute of Technology (2013) developed a quadcopter with folding arm structure [43]. The UAV's result was 800 meters and found with a slight break in the landing situation. The authors of this paper have participated in 2016, 2017, and 2018 as UAVs in the type of quadcopter. At the time of participation in 2016, the organization of the quadcopter structure was not optimized [44]. For example, the total weight of the UAV was over 973 grams due to the two batteries and the high weight of the components. The UAV has the distance error of 1,329 meters with most of the body was damaged. In 2017, we had completed the optimized UAV structure with 524 grams with a single battery and light components based on our experience in 2016 [16]. However, it did not use optimized flight algorithms, resulting in 1,800 meters result due to a lack of batteries. In 2018, we developed an optimizing flight algorithm for the structure developed in 2017. The UAV achieved a record of 81 meters. The results of all the teams participating in the ARLISS competition are listed on Table 4. The results of the experiments proposed in this paper show the smallest distance error.

V. CONCLUSION

This study developed a method to extend the operational time and flight distance of quadcopters, which operate on limited battery capacity. The method consists of a high-altitude flight initiation system that uses a carrier rocket, as well as an autonomous ramp flight algorithm. First, the carrier rocket's energy was consumed as the rocket flew to a preset altitude and distance. Then, the quadcopter was ejected from the carrier rocket, initiated high-altitude flight, and autonomously flew to the target point. To achieve this goal, we used a folding mechanism that employs a foldable structure to load the quadcopter into the carrier rocket, which has a limited volume. We also used an autonomous flight algorithm that follows a flight path on a slope to get to the target point by taking the shortest route. To verify the high-altitude flight initiation system at a height of 3 km, experiments were performed at the ARLISS competition held in the desert in Nevada, US. The mission quadcopter's real-time latitude, longitude, and altitude information were stored in the EEPROM within the main controller. The stored GPS-based information was used to check the position information of the quadcopter's flight trajectory. The mission quadcopter's ramp flight distance was 0.71 km. The position error between the preset target point and the actual landing point of the mission quadcopter is 0.08km. It is regarded as an acceptable result considering the high flight initiation altitude of 1.28 km and the serve desert environment with strong wind and dust. The high-altitude flight initiation system and autonomous ramp flight algorithm developed in this study can be used in the future in a variety of fields where it is necessary to take off/land from/to moving objects such as planes, rockets, and maritime launch services. The autonomous flight algorithm proposed in this paper was performed in an environment without obstacles. However, there are limitations in applying it to practical applications where it is usual that there are many obstacles. Therefore, in the future, we plan to research advanced algorithms that perform avoidance control through recognition and judgment of obstacles and terrain using vision and various sensors with sophisticated algorithms e.g. artificial intelligence.

REFERENCES

[1] M. Hassanalian, D. Rice, and A. Abdelkefi, "Evolution of space drones for planetary exploration: A review," *Prog. Aerosp. Sci.*, vol. 97, pp. 61–105, Feb. 2018.

[2] I. Colomina and P. Molina, "Unmanned aerial systems for photogrammetry and remote sensing: A review," *ISPRS J. Photogramm. Remote Sens.*, vol. 92, pp. 79–97, Jun. 2014.

[3] D. Floreano and R. J. Wood, "Science, technology and the future of small autonomous drones," *Nature*, vol. 521, no. 7553, pp. 460–466, May 2015.

[4] K. Anderson and K. J. Gaston, "Lightweight unmanned aerial vehicles will revolutionize spatial ecology," *Frontiers Ecol. Environ.*, vol. 11, no. 3, pp. 138–146, Apr. 2013.

[5] S.-H. Kim, D.-K. Lee, J.-H. Cheon, S.-J. Kim, and K.-H. Yu, "Design and flight tests of a drone for delivery service," *J. Inst. Control, Robot. Syst.*, vol. 22, no. 3, pp. 204–209, Mar. 2016.

[6] S. Gupte, P. Infant Teenu Mohandas, and J. M. Conrad, "A survey of quadrotor unmanned aerial vehicles," in *Proc. IEEE Southeastcon*, Mar. 2012, pp. 1–6.

[7] H. Jeaong, S. Jo, J. Suk, S. Kim, Y.-G. Lee, and I. Chung, "Modeling of aerodynamic database and robust control using disturbance observer for quadcopter," *J. Inst. Control, Robot. Syst.*, vol. 24, no. 6, pp. 519–531, Jun. 2018.

[8] H. Chao, Y. Cao, and Y. Chen, "Autopilots for small unmanned aerial vehicles: A survey," *Int. J. Control, Autom. Syst.*, vol. 8, no. 1, pp. 36–44, Feb. 2010.

[9] J. Lee and T. Jin, "Tracking of walking human based on position uncertainty of dynamic vision sensor of quadcopter UAV," *J. Inst. Control, Robot. Syst.*, vol. 22, no. 1, pp. 24–30, Jan. 2016.

[10] A. M. Jawad, H. M. Jawad, R. Nordin, S. K. Gharghan, N. F. Abdullah, and M. J. Abu-Alshaeer, "Wireless power transfer with magnetic resonator coupling and Sleep/Active strategy for a drone charging station in smart agriculture," *IEEE Access*, vol. 7, pp. 139839–139851, 2019.

[11] M. Lu, M. Bagheri, A. P. James, and T. Phung, "Wireless charging techniques for UAVs: A review, reconceptualization, and extension," *IEEE Access*, vol. 6, pp. 29865–29884, 2018.

[12] J. Park, H. Lee, S. Eom, and I. Lee, "UAV-aided wireless powered communication networks: Trajectory optimization and resource allocation for minimum throughput maximization," *IEEE Access*, vol. 7, pp. 134978–134991, 2019.

[13] F. Wu, D. Yang, L. Xiao, and L. Cuthbert, "Energy consumption and completion time tradeoff in rotary-wing UAV enabled WPCN," *IEEE Access*, vol. 7, pp. 79617–79635, 2019.

[14] S.-I. Higashino, M. Hayashi, S. Nagasaki, S. Umemoto, and M. Nishimura, "A balloon-assisted gliding UAV for aerosol observation in antarctica," *Trans. Jpn. Soc. Aeronaut. Space Sci., Aerosp. Technol. Jpn.*, vol. 12, pp. a35–a41, 2014.

[15] S. Jo, B. Lee, J. Oh, J. Song, C. Lee, S. Kim, and J. Suk, "Experimental study of in-flight deployment of a multicopter from a fixed-wing UAV," *Int. J. Aeronaut. Space Sci.*, vol. 20, no. 3, pp. 697–709, Sep. 2019.

[16] C. Lee, K. N. I. o. T. Department of Mechanical System Engineering, and B. Chu, "Autonomous flight experiment of a foldable quadcopter with airdrop launching function," *Korean Soc. Manuf. Process Eng.*, vol. 17, no. 2, pp. 109–117, Apr. 2018.

[17] C. Lee, H. Kang, and B. Chu, "Airdrop operation and autonomous flight-back experiment of dual unmanned aircraft," *J. Inst. Control, Robot. Syst.*, vol. 25, no. 6, pp. 519–525, Jun. 2019.

[18] ARLISS. *CanSat Satellite Project*. Accessed: Dec. 18, 2019. [Online]. Available: http://www.arliss.org

[19] University of Nevada. *Reno Engineering*. Accessed: Dec. 18, 2019. [Online]. Available: https://www.rgj.com/story/news/2014/09/08/unr-teamcompeting-battle-drones/15288115

[20] S. Nakasuka, Y. Nakamura, R. Funase, M. Nagai, and R. Kawashima, "Autonomous parafoil control experiment as 'Comeback competition' for effective first step training towards satellite development," *IFAC Proc. Volumes*, vol., 37, no. 6, pp. 919–924, 2004.

[21] J. C. LaCombe, E. L. Wang, M. Nicolescu, P. Rivera, and B. Poe, "Design experiences with a student satellite program," in *Proc. Amer. Soc. Eng. Educ. Pacific Southwest Annu. Conf.*, 2007, pp. 1–10.

[22] S. Yamaura, H. Akiyama, and R. Kawashima, "Report of CanSat leader training program," in *Proc. 5th Int. Conf. Recent Adv. Space Technol. (RAST)*, Jun. 2011, pp. 856–860.

[23] R. Kawashima, "CanSat leader training program: Past, present and future," *Ciencia UANL*, vol. 19, no. 81, pp. 76–82, 2016.

[24] *Seoul National University Satellite Team*. Accessed: Dec. 18, 2019. [Online]. Available: https://snusat.wordpress.com

[25] S. Nakasuka, "Students' challenges towards new frontier-enlarging activities of UNISEC and Japanese Universities," *Trans. Jpn. Soc. Aeronaut. Space Sci., Space Technol. Jpn.*, vol. 7, no. 26, pp. 1–16, 2009.

[26] J. Park, "Bring-back cansat mission for a simulated resupply mission on a remote planet," in *Proc. KSAS*, 2014, pp. 1516–1518.

[27] MultiWii. *General Purpose Software to Control a Multirotor RC Model*. Accessed: Dec. 18, 2019. [Online]. Available: https://code.google.com/archive/p/multiwii/

[28] S. Mintchev and D. Floreano, "A pocket sized foldable quadcopter for situational awareness and reconnaissance," in *Proc. IEEE Int. Symp. Saf., Secur., Rescue Robot. (SSRR)*, Oct. 2016, pp. 396–401.

[29] B.-S. Yu, H.-D. Kim, C.-R. Lee, and S.-K. Kim, "Auto-tuning quadcopter attitude control based-on steepest gradient method," *J. Inst. Control, Robot. Syst.*, vol. 24, no. 10, pp. 924–929, Oct. 2018.

[30] G. Hong, "Linear controllable systems," *Nature*, vol. 135, no. 5, pp. 18–27, 1990.

[31] R. Baker, "Nonlinear unstable systems," *Int. J. Control*, vol. 23, no. 4, pp. 123–145, 1989.
[32] K. Hong and C. Kim, "Linear stable systems," *IEEE Trans. Autom. Control*, vol. 33, no. 3, pp. 1234–1245, Dec. 1993.
[33] Y. Mam, *The Technical Writer's Handbook*. Mill Valley, CA, USA: Univ. Science, 1989.
[34] D. Deb, G. Tao, J. O. Burkholder, and D. R. Smith, "Adaptive synthetic jet actuator compensation for a nonlinear aircraft model at low angles of attack," *IEEE Trans. Control Syst. Technol.*, vol. 16, no. 5, pp. 983–995, Sep. 2008.
[35] R. Patel, D. Deb, H. Modi, and S. Shah, "Adaptive backstepping control scheme with integral action for quanser 2-dof helicopter," in *Proc. Int. Conf. Adv. Comput., Commun. Informat. (ICACCI)*, Sep. 2017, pp. 571–577.
[36] D. Viswanath, S. Krishnaswamy, and D. Deb, "Homing missile guidance using LOS rate and relative range measurement," in *Proc. Annu. IEEE India Conf. (INDICON)*, Dec. 2015, pp. 1–6.
[37] D. Kapoor, D. Deb, A. Sahai, and H. Bangar, "Adaptive failure compensation for coaxial rotor helicopter under propeller failure," in *Proc. Amer. Control Conf. (ACC)*, Jun. 2012, pp. 2539–2544.
[38] ARLISS2012. *CanSat Satellite Project*. Accessed: Aug. 7, 2020. [Online]. Available: http://www.unisec.jp/history/arliss2012/report/NASU_pre.pdf
[39] ARLISS2013. *CanSat Satellite Project*. Accessed: Aug. 7, 2020. [Online]. Available: http://www.unisec.jp/history/arliss2013/report/09_tby_pre.pdf
[40] ARLISS2010. *CanSat Satellite Project*. Accessed: Aug. 7, 2020. [Online]. Available: http://unisec.jp/history/arliss2010/report/soka_pre.pdf
[41] A. J. Smith, "Aerial deployed unfolding autonomous glider system," in *Proc. 53rd AIAA Aerosp. Sci. Meeting*, Jan. 2015, p. 0374.
[42] ARLISS2018. *CanSat Satellite Project*. Accessed: Aug. 7, 2020. [Online]. Available: http://www.t.u-tokyo.ac.jp/foee/topics/setnws_20180920175651688564908O.html
[43] A. AlSaibie, A. Kivila, J. Pottre, and W. Singhose, "Fostering global collaboration between engineering students through a robotic design competition," in *Proc. Hawaii Univ. Int. Conf. Sci., Technol., Eng., Math Educ.*, 2014, pp. 1–8.
[44] ARLISS. (2016). *Kumoh National Institute of Technology*. Accessed: Aug. 27, 2020. [Online]. Available: https://irobot.kumoh.ac.kr/Folding-Autonomous-QuadCopter
[45] ARLISS. *CanSat Satellite Project*. Accessed: Aug. 7, 2020. [Online]. Available: https://docs.google.com/viewerng/viewer and https://www.aeropac.org//images/CanSatRegulation_byUNISEC_2018_ver1.pdf

CHEONGHWA LEE received the B.S. and M.S. degrees in mechanical engineering from the Kumoh National Institute of Technology, Gumi-si, Gyeongsangbuk-do, South Korea, in 2017 and 2019, respectively. He is currently pursuing the Ph.D. degree in electrical and computer engineering with Seoul National University, Seoul, South Korea. He was a Research Assistant with the Korea Institute of Industrial Technology, Yeongcheon-si, Gyeongsangbuk-do. His current research interest includes artificial intelligence-based robotic automation control and applications.

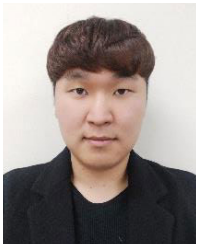

SANGWOONG LEE received the B.S. degree from the Department of Mechanical System Engineering, Kumoh National Institute of Technology, in 2019, where he is currently pursuing the M.S. degree. His research interest includes robotics.

BAEKSUK CHU received the B.S., M.S., and Ph.D. degrees in mechanical engineering from Korea University, in 1999, 2001, and 2006, respectively. He joined the Kumoh National Institute of Technology, in 2001, where he is currently an Associate Professor with the Department of Mechanical System Engineering. His current research interests include robotics, mechatronics, intelligent control, and reinforcement learning.